Controlling system components with a sound card: A versatile inkjet fluid testing platform

Brice Bognet, Yang Guo, and Anson W. K. Ma

Articles you may be interested in

The production of monodisperse explosive particles with piezo-electric inkjet printing technology
Rev. Sci. Instrum. **86**, 125114 (2015); 10.1063/1.4938486

Jetted mixtures of particle suspensions and resins
Phys. Fluids **26**, 101701 (2014); 10.1063/1.4897238

The impulse response of a high-speed jet forced with localized arc filament plasma actuators
Phys. Fluids **24**, 125104 (2012); 10.1063/1.4772191

Breakup of diminutive Rayleigh jets
Phys. Fluids **22**, 122003 (2010); 10.1063/1.3524533

Atomization patterns produced by the oblique collision of two Newtonian liquid jets
Phys. Fluids **22**, 042101 (2010); 10.1063/1.3373513
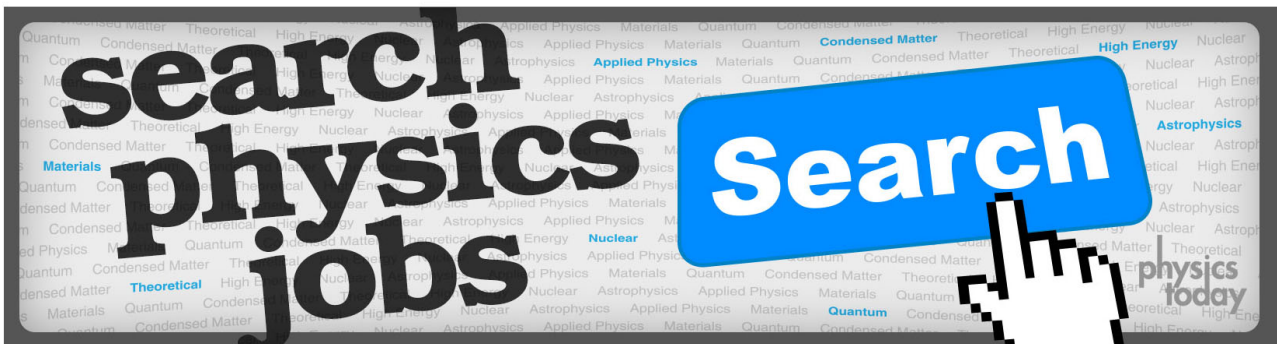
Controlling system components with a sound card: A versatile inkjet fluid testing platform

Brice Bognet,[1] Yang Guo,[1] and Anson W. K. Ma[1,2,a]

[1]Polymer Program, Institute of Materials Science, University of Connecticut, Storrs, Connecticut 06269, USA
[2]Department of Chemical and Biomolecular Engineering, University of Connecticut, Storrs, Connecticut 06269, USA

In this paper, we demonstrate how to use a personal computer sound card to develop an experimental platform for evaluating the jettability and jetting behavior of inkjet fluids. The test fluid is driven out of a nozzle acoustically using a loudspeaker, forming a jet. The subsequent jet breakup process is then captured using a stroboscopic light source and a camera. Instead of using a delay generator as in previous work, the current setup uses a computer sound card and audio amplifier to (i) generate actuation waveforms of arbitrary shapes and (ii) synchronize the jet actuation and imaging with a time precision close to 5 μs. To correct for any signal distortions caused by the built-in high pass filters of the sound card and amplifier, a numerical filter is created and applied before sending the desired signal to the sound card. Such correction method does not require physically modifying the hardware of the sound card or amplifier and is applicable to different waveforms and filters provided that the transfer function is correctly identified. The platform has been tested using 20% (v/v) glycerol in water as a model fluid. Combining this platform with digital image analysis further enables a quantitative assessment of parameters such as the volumes and positions of the jet and drop that are important for quality control and development of new ink formulations. © 2016 AIP Publishing LLC. [http://dx.doi.org/10.1063/1.4939043]

I. INTRODUCTION

Inkjet printing has emerged from a method for producing bar codes and graphic arts to a digital fabrication technique capable of patterning a wide range of materials such as metallic and inorganic particles, ceramic, and biomaterials.[1] Inkjet printing is a maskless, non-contact printing method offering advantages in terms of speed, versatility, scalability, and minimal material usage. For electronic applications, conductive inks are usually made up of conducting particles suspended in a carrier fluid with the aid of a dispersant. The carrier fluid is removed after drop deposition, and the particles may be further sintered to increase conductivity. Inkjet printing also forms the basis of 3D printing methods such as PolyJet™, ProJet™, and ZPrinter™. These methods are based on printing (i) photo-curable resins and wax support materials or (ii) a binder onto a powder bed. For biomedical applications, cells and hydrogels may be printed to form "organs-on-a-chip" and 3D cell cultures for drug screening and regenerative medicine applications.[2,3] Most importantly, there is a strong and growing demand for characterizing the fluid properties as material scientists continue to develop and formulate new functional materials for inkjet and inkjet-based 3D printing. The reliability of inkjet printing strongly depends on the spread of the drop size distribution and directionality as the drop travels, while the smallest drop size, together with the contact angle, affects the drop footprint and resolution.[4] Fundamentally, the viscoelasticity and surface tension of the printing fluids modify the jet breakup and the drop formation process driven by Plateau-Rayleigh instability. Such instability may also lead to the formation of small "satellite" drops, which further result in drop size variation and thus are generally considered to be undesirable.[5–7]

Capillary and torsional rheometers are commercially available to measure the high-shear viscosities (up to 10^5 s^{-1}) and viscoelasticity of ink fluids. However, the actuation frequency experienced by the fluid in a piezoelectric print head, for example, is orders of magnitude higher (10−30 kHz) and the residence time orders of magnitude shorter than that accessible by a commercial rheometer.[8,9] Imaging the jet and drop formation during printing offers a more direct way of evaluating the jettability of ink fluids. High-speed and stroboscopic imaging techniques have been developed and applied by several research groups to visualize the jetting and subsequent drop formation and impact on a substrate.[10–14] These imaging platforms are instrumental in the fundamental studies of different types of inks and their jettability. However, these platforms also require a delay generator to synchronize the actuation and imaging actions, and the actuation is limited to rather simple waveforms, such as sinusoidal and square.

In this paper, we report a novel, versatile inkjet fluid testing platform for quality control and the quick screening of new ink formulations. The platform is based on the built-in sound card of a computer instead of a delay generator. Sound cards are often used to record signals,[15–19] but are rarely used to generate signals other than simple waveforms for a frequency higher than 20 Hz[20] because of signal distortions at lower frequencies caused by the built-in high pass filters. We overcome this limitation without modifying the hardware

a)anson.ma@uconn.edu

of the sound card. The resulting imaging platform was tested using a mixture of water-glycerol as a model fluid.

The drops in this paper are generated acoustically and have a volume on the order of hundreds of microliters—orders of magnitude larger than those typically found in commercial inkjet systems. Current state-of-art liquid dispensing technologies, such as pyroelectrodynamic shooting,[21] electrodynamic jet printing,[22] surface pre-patterning,[23] and certain non-standard inkjet methods,[24] allow the patterning of drops with a volume in the nano- and even atto-liters range. In principle, the concept of using a sound card to synchronize the jetting and imaging may be extended to other printing systems with appropriate configuration and optics.

II. EXPERIMENTAL DETAILS

A. Drop generator and imaging platform

The inkjet fluid testing platform described in this paper was inspired by the work of Castrejón-Pita et al.[10] The platform is composed of a drop generator, a CMOS camera (2048 × 1088, 2 MPix IDS 3360 CP), a macro-lens (NAV-ITAR), and a stroboscopic light source (Shimpo DT-326 Portable LED Stroboscope). The method used to trigger the camera and the light source will be explained in Sec. II B. The drop generator consists of a chamber with a fluid intake and a 1-mm nozzle facing down. The test fluid contains 20% (v/v) glycerol (Reagent ACS, 99.6%, ACROS Organics) in water.

The top of the chamber is made up of a brass membrane, which is further attached to a loudspeaker (4 or 8 Ω). Liquid jets or drops are created acoustically by sending a trigger signal to the loudspeaker. The displacement of the loudspeaker membrane is correlated with the electric current. As the voltage increases, the current increases, and consequently, the membrane generates a positive displacement and pressure wave. The liquid chamber is well sealed, so when the voltage decreases, the membrane generates a negative pressure, pulling the meniscus inside the chamber. A schematic diagram of the experimental device is shown in Fig. 1(a). Fig. 1(b) shows the actual imaging platform and Fig. 1(c) shows two different designs of the nozzle plate. The slight protrusion helps to prevent nozzle plate flooding while the low aspect ratio reduces the chance of nozzle clogging.[1,25,26] An alternative design has a Luer lock fitting where syringe needles with different gauges (inner diameter: 80 μm–4.39 mm) can be attached as a changeable nozzle.

### B. Synchronization between actuation and imaging

Unlike Refs. 13 and 14, a high-speed camera is not used, and as a result, the camera and the drop generating signal must be synchronized to capture images of the liquid jet and drops. The light source and the camera are both triggered by the same signal. Another signal is sent to the loudspeaker to generate a pressure wave in the chamber and consequently a liquid jet. One way to synchronize those signals is to use a delay generator as in Ref. 10. However, the use of a delay generator requires adjusting the delay progressively to record an image at a different time relative to the drop generating
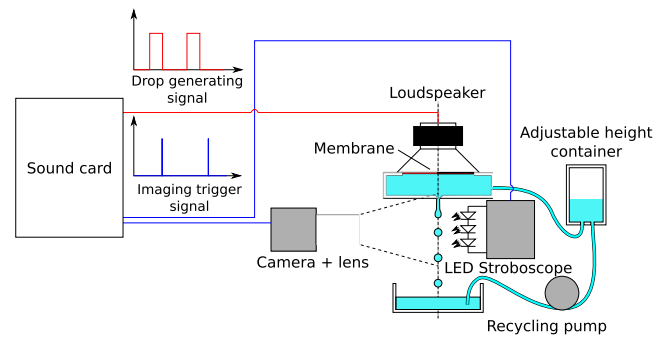
(a) Schematic diagram
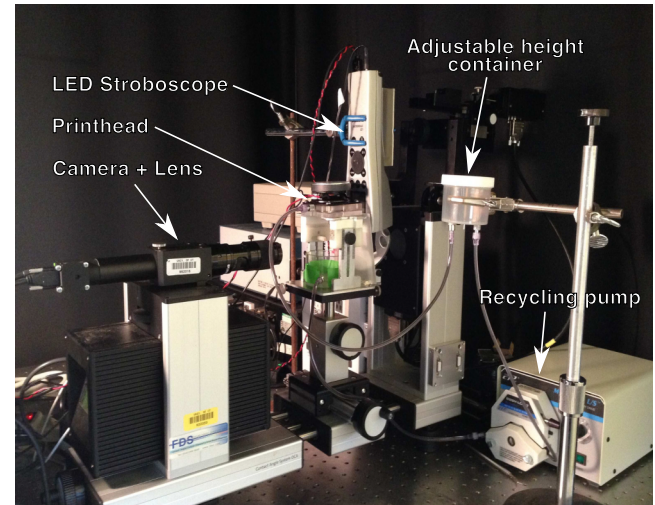
(b) Actual experimental platform.
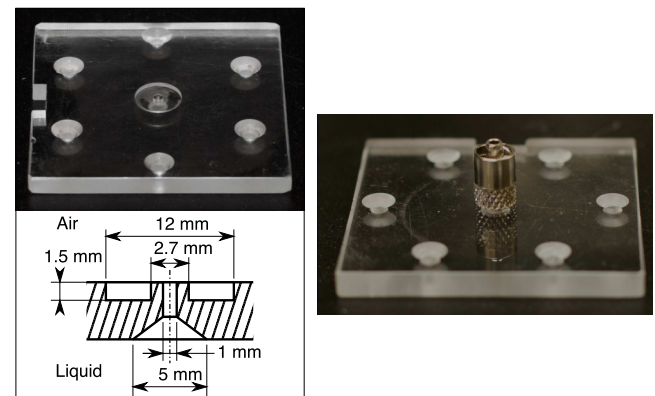
(c) Changeable nozzle / Luer Lock designs

FIG. 1. Overview of the sound card-based inkjet fluid testing system.

trigger. In Ref. 10, a relay is triggered by the delay generator and a square drop-generating signal is generated. The use of a sound card allow to generate arbitrary waveform easily instead of a square signal only.

In this paper, a sound card is used to generate the trigger signals for both imaging and drop generation, offering versatility and simplicity. The stereo nature of the sound card allows the triggering of both the imaging and drop-generation signals with good time precision. Most sound cards can generate signals at a sampling rate between 44 kHz and 196 kHz. At 196 kHz, the time resolution is close to 5 μs. More sophisticated sound cards with up to 6 channels are readily available in surround sound audio systems. Although only

two channels are used in the current paper, the extra channels offer even more flexibility to control and synchronize any additional instruments (e.g., deflection plates as in continuous inkjet (CIJ) printing). Depending on the maximum output voltage of the sound card, an audio amplifier may be needed. BEHRINGER EPX4000 is used in the current paper. A stereo signal is generated with one channel connected to the loudspeaker and the other one to the camera and light source. A delay between the drop generation and image capturing can be achieved by sending signals with slightly different frequencies (Fig. 2). This way, a large number of frames may be recorded without the need to adjust the delay time systematically as in the case of a delay generator.

## C. Waveform control–correction of the signal

Matlab® software was used to create an audio file that controls the inkjet platform and imaging. The file can be played using any media player software (VLC http://www.videolan.org, for example). This method allows the creation of any shape of waveforms (see, for example, Fig. 3) and thus offers more versatility compared to using a function generator. Using this platform, the printing consistency of the jetting can be easily assessed by taking images of different drops at the same delay time between the drop actuation and imaging (Fig. 2). This platform may be further used to optimize the actuation waveform for different inkjet fluids and various print head designs in terms of jetting consistency and satellite drop formation.

Both the sound card and the amplifier contain a first-order high-pass filter designed to remove any direct current (DC) components or biases of the signals, thereby minimizing the current running through the loudspeakers and the associated heat generation. These filters, however, also cause the attenuation of any low frequency components of the signals, leading to the distortion of the output signals (Fig. 4).
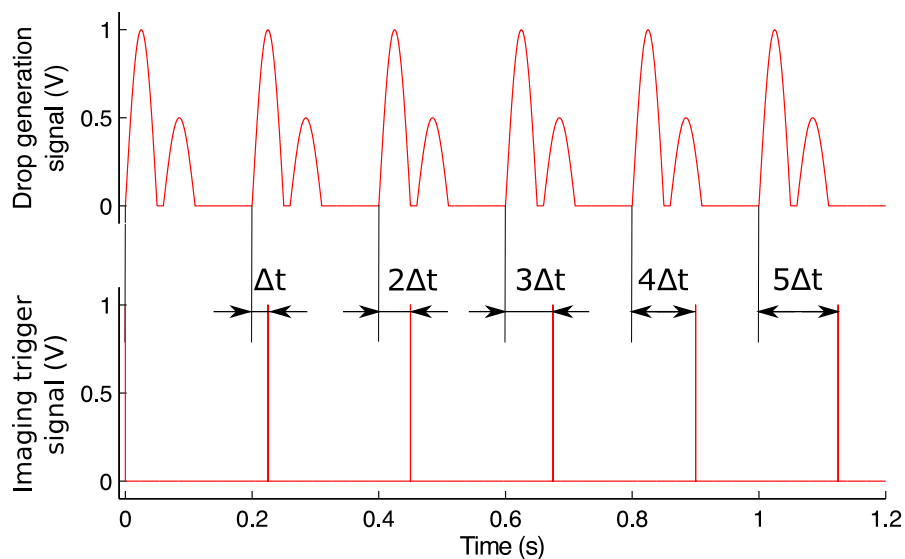
(a) One image per delay time
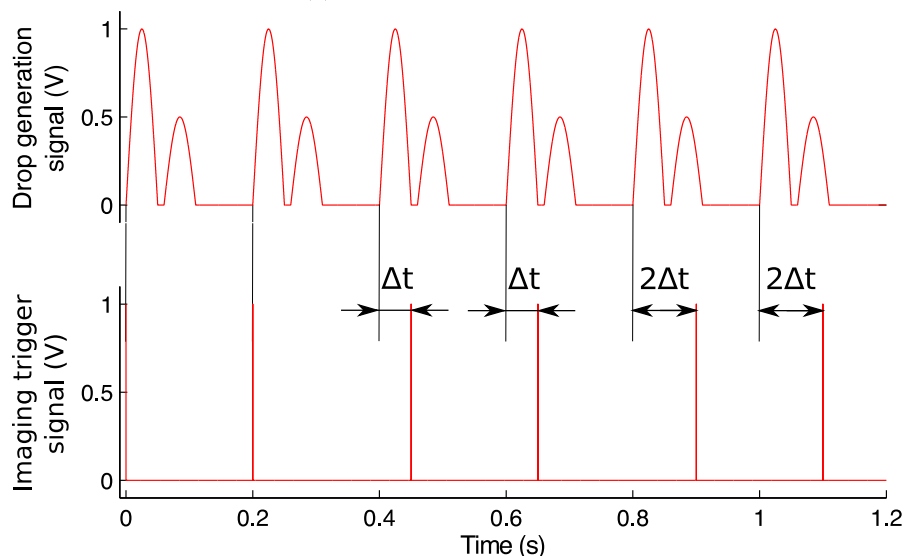
(b) Two images per delay time

FIG. 2. Drop generation and imaging trigger signals at different frequencies are used to adjust the delay time (Δt) between the drop generation and image capturing and to control the number of images taken for a given delay time.

(a) One positive sine wave

(b) Two positive sine wave

(c) One positive exponential wave

(d) Two positive exponential waves

(e) One positive square wave
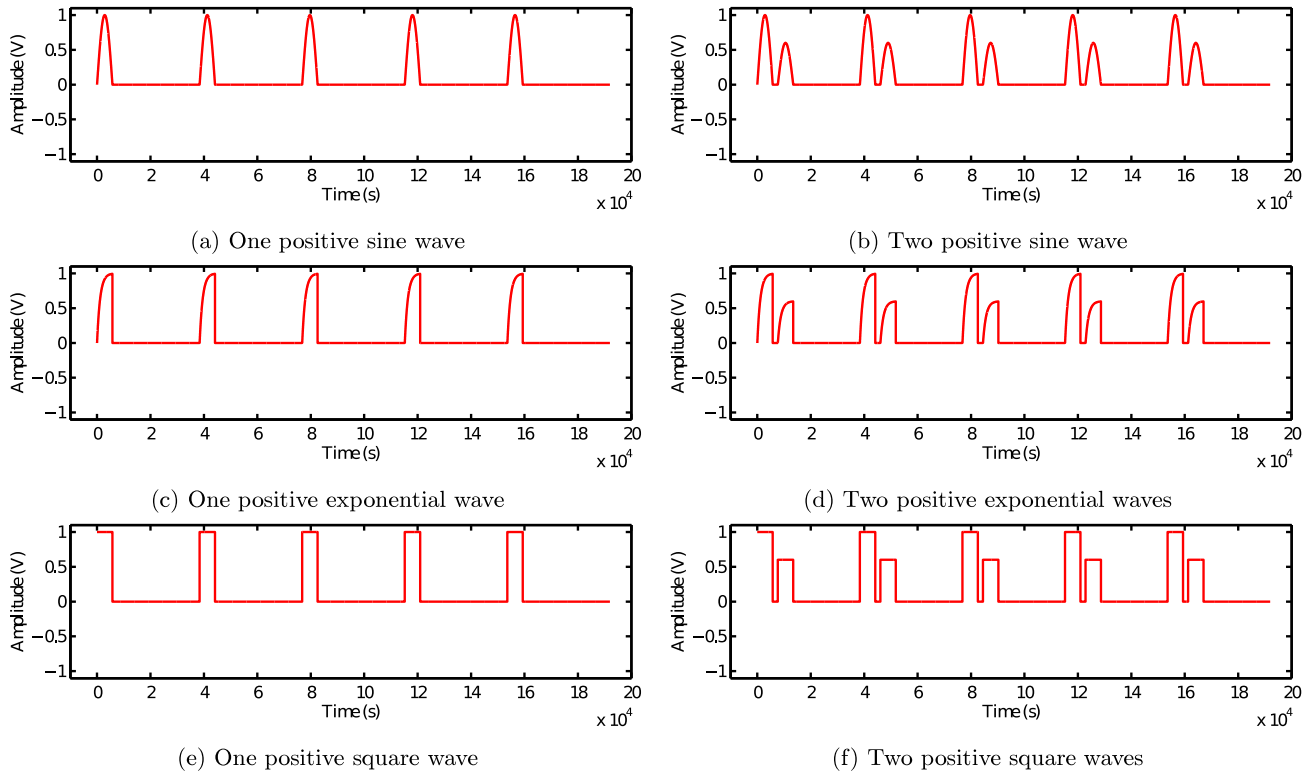
(f) Two positive square waves

FIG. 3. Sample drop generating signals created as an audio file using Matlab®.

Such degeneration is especially detrimental to using sound card for drop generation because the relevant frequencies for the current drop generator are from 5 to 50 Hz, lower than the audible frequencies (20 Hz–20 kHz).

D. High-pass filters characterization

To compensate for the effects of the built-in high-pass filters in both the sound card and amplifier, a numerical filter is created and then applied to modify the input signal to the sound card (Fig. 5). First, the characteristics of the high-pass filter of the sound card are identified by sending sinusoidal waves with a constant amplitude to the sound card. The output

voltage of the signal is then measured using an oscilloscope. A Bode magnitude plot of the filter is produced by repeating the measurement and varying the frequency of sinusoidal waves from 1 Hz to 10 kHz (Fig. 6). The experimentally determined Bode plot is then fit by assuming a first-order high-pass filter, where the transfer function is given as

$$H_{\text{soundcard}}(s) = \frac{s}{\omega_{0_1} + s}, \qquad (1)$$

where s is the Laplace domain variable. The best fit value of the cutoff frequency in this example is $\omega_{0_1} = 0.040$ rad/s.

The inverse transfer function $\frac{1}{H_{\text{sound card}}(s)}$ is applied to the input signal to the sound card using the Matlab®

(a) Desired signal
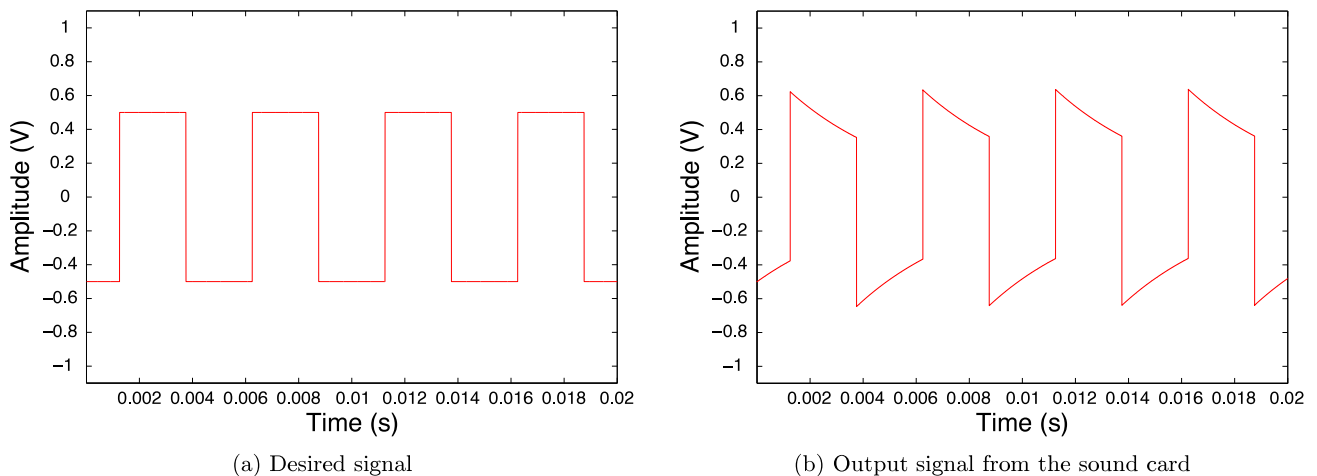
(b) Output signal from the sound card

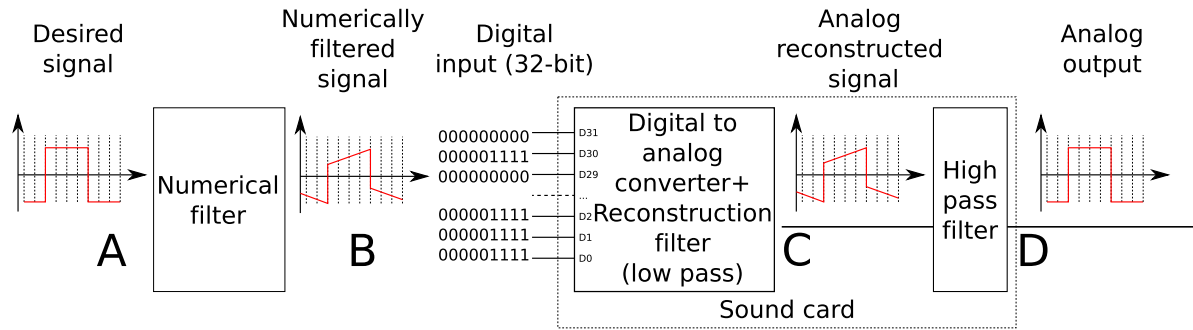FIG. 4. Desired signal and output signal from the sound card without the numerical filter.

FIG. 5. Block diagram of the signal generation. A numerical filter is applied to correct for any signal distortions caused by the built-in high-pass filters of the sound card and amplifier (not shown).

control system toolbox. The toolbox simulates the temporal response of any transfer functions and acts as a numerical filter, boosting the low frequencies and compensating for any attenuation caused by the physical high-pass filter of the sound card. The procedure should then be repeated to rectify any signal distortion caused by the high-pass filter of the amplifier. To measure the characteristics of the filter in the amplifier, the preconditioning filter $\frac{1}{H_{\text{sound card}}(s)}$ is used to output a sinusoidal wave with a constant amplitude from the sound card (input of the amplifier).

Fig. 7 shows the Bode plot associated with the high-pass filter of the amplifier.

The first-order filter for the amplifier is modeled as

$$H_{\text{amplifier}}(s) = \frac{s}{\omega_{0_2} + s}. \qquad (2)$$

The best-fit value of the cutoff frequency of the amplifier is $\omega_{0_2} = 0.037$ rad/s.

E. Preparing the signal

Once the characteristics of the high-pass filters of the sound card and the amplifier are identified, the input signal is processed with the corresponding inverse transfer functions,

$$H_{\text{preconditioning}}(s) = \frac{1}{H_{\text{sound card}}(s)} \frac{1}{H_{\text{amplifier}}(s)}. \qquad (3)$$

The exact cutoff frequency of the filters may vary depending on the actual sound card and amplifier used. The inverse transfer function of two first-order high-pass filters connected in series features a positive gain at low frequencies, which is the characteristic of an active filter (Fig. 8). However,

this imposes no constraints because a numerical filter instead of a physical filter is used.

As shown in Fig. 5, after the numerical filter correction, the actual output signal is the same as the desired output signal. The numerical filter correction method is not limited to sinusoidal waves and can be applied to signals with arbitrary shapes because any signals can be represented by a combination of sinusoidal waves. More importantly, this method does not require any physical modification of the hardware and therefore is robust and easy to apply.

III. IMAGE ANALYSIS

A. Contour detection and useful numbers

As an example, a cosine function (Fig. 10(a)) is used as the actuation signal

$$V_D = \begin{cases} V_0(1 - \cos(\omega t)) & t \in [0; \pi/\omega] \\ 0 & t \in [\pi/\omega; t_f] \end{cases}, \qquad (4)$$

where $V_0 = 15$ V, $t_f = 0.04$ s, and $\omega = \pi/0.006$ s^{-1}. The baseline value of this signal was chosen to ensure the output signal from the numerical filter (point B in Fig. 5) was periodic and bounded (see Section IV). For this experiment, 10 images were recorded at the same delay time for evaluating the consistency of the jetting. Stroboscopic imaging follows different drops at different times after jetting. If the jetting is consistent, the entire sequence of jetting can be reconstructed (Fig. 9(a)). Further, the contour of the jet and any drop at a given time can be detected from the images using a gradient-based method as reported in Refs. 27 and 28. After the contour detection, a binary image was generated for each original image (Fig. 9(b)). The binary images were then used
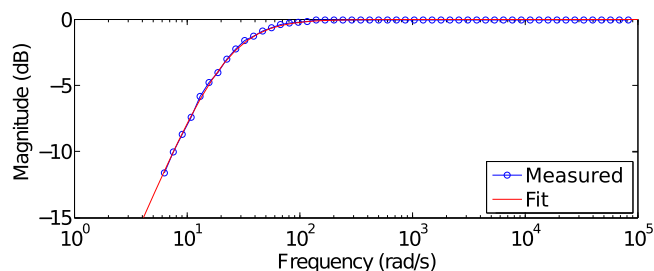

FIG. 6. Bode magnitude plot of the experimentally measured output of the sound card and the corresponding fit by assuming a first-order transfer function.
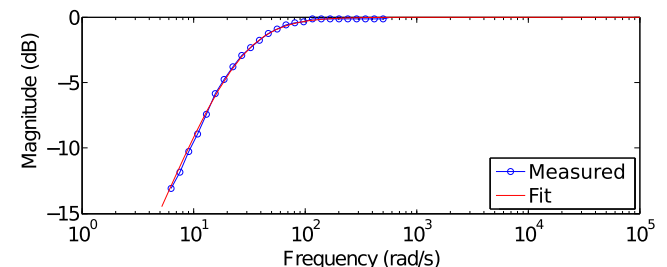

FIG. 7. Bode magnitude plot of the experimentally measured output of the amplifier and the corresponding fit by assuming a first-order transfer function.
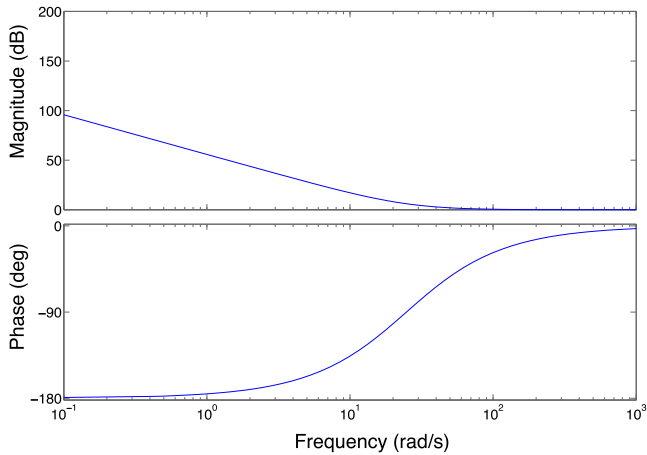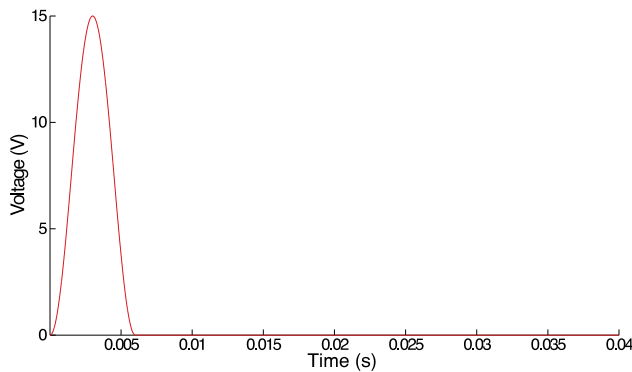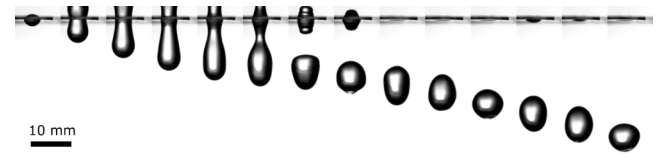
FIG. 8. Bode plot of the numerical filter created based on the inverse transfer functions associated with the sound card and amplifier.


(a) Original images

(b) Binary images

FIG. 9. Reconstructed time evolution of a water-glycerol jet in air generated using a cosine signal as shown in Fig. 10.

to calculate the positions of the tip of the jet, the front, the rear, and the center of the drop detached from the jet, as well as the jet and drop volumes (Fig. 10(b)). Error bars in Fig. 10(c) represent the standard deviations of the positions based on 10 images. As shown in the figure, the variation is relatively small—on the order of 55 μm for the drop center position, for example. The volume of the jet and the droplets were calculated by assuming axisymmetry. The flow rate through the nozzle at a given time was calculated from the time derivative of the computed volume of the jet (Fig. 10(d)).

A positive flow rate indicates that the jet is ejected from the nozzle, whereas a negative flow rate occurs as the jet retracts into the nozzle. Other information, such as the break-up time at which a drop was separated from the jet and the volume of the drop, was also obtained from the captured images (Table I). More importantly, one can conveniently perform a statistical analysis to evaluate the jetting consistency for a given ink formulation and print head.

IV. LIMITATIONS AND IMPROVEMENTS

The sound card-based platform has been demonstrated using a drop-on-demand (DoD) printing mode. The setup

(a) Drop generating signal

(b) Jet and drop positions
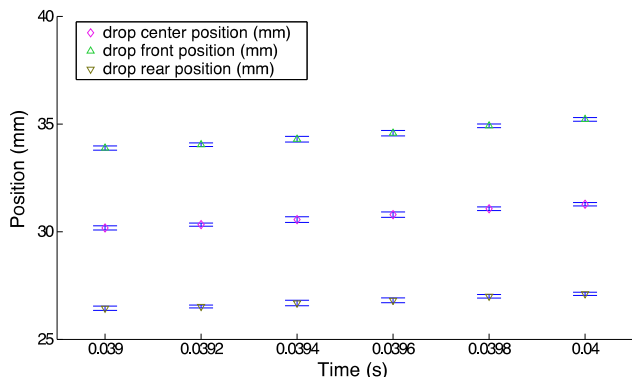
(c) Jet and drop positions. Error bars show the standard deviations calculated based on 10 images at a given time
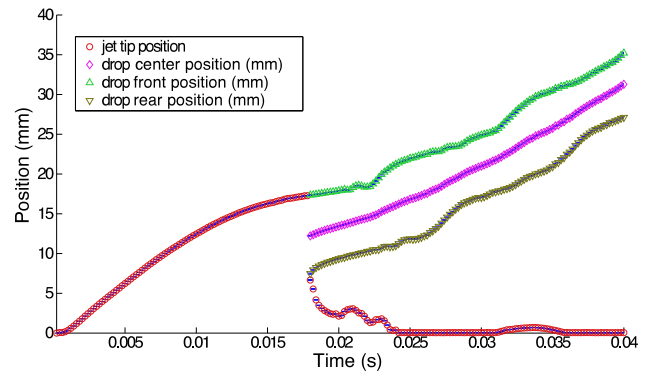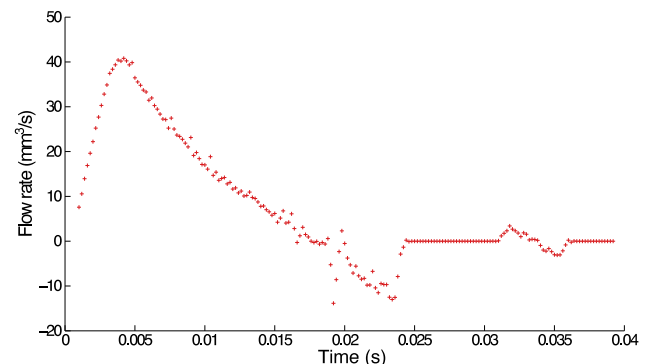
(d) Average flow rate through the nozzle calculated based on 10 images for a given delay time

FIG. 10. Sample data collected from image analysis.

TABLE I. Jet breakup time and volume of the detached drop.

	Average	Standard deviation
Breakup time (ms)	18	0.1
Drop volume (μl)	266	6.31

can be easily reconfigured to CIJ mode.[10] The rheological response of a fluid strongly depends on the characteristic time scale of the process relative to the characteristic time scale of the fluid. The accessible process time scale of the current setup is limited by the sampling rate of the sound card and inertia of the acoustic system. The time resolution and the baseline voltage of the signals generated based on the sound card are largely limited by the technical specifications of the sound card. The maximum time resolution of a 196 kHz sound card is on the order of 5 μs, which is much lower than that of a delay generator capable of resolving 10 ns. Some high-quality audio devices (http://antelopeaudio.com) on the market can generate sound at a sampling rate as high as 384 kHz, corresponding to a time resolution of 2.6 μs. Higher time precision may be achieved as the sound card technology improves in the future. A stereo sound card with two channels was used in this paper. However, sound cards with six channels (i.e., 5.1 sound cards) are also readily available, allowing the simultaneous control of more components. In terms of imaging, the setup may be integrated with a high-speed camera[28] to follow the evolution of the same jet and drop rather than different drops. The sharpness of the images can be further improved using a digital single-lens reflex (DSLR) camera with high-quality optics.

Part of the output signal from the numerical filter (point B in Fig. 5) is a time integral of the target signal as shown in Figs. 11(a) and 11(b). If the target signal does not have a negative voltage, then the output signal of the numerical filter will continue to increase over time until it reaches the maximum output voltage of the sound card. Likewise, if the target signal does not have a positive voltage, the output voltage of the numerical filter will decrease over time, reaching the minimum working voltage of the sound card. The time duration over which the numerical filter can be applied is limited as a result. In this paper, a loudspeaker was used to generate a pressure wave in the print head by converting the electrical signals to membrane displacements. The displacement of the membrane depends

(a) Desired signal (Point A in Figure 5), zero baseline

(b) Output signal from the numerical filter (Point B in Figure 5)

(c) Desired signal (Point A in Figure 5), non-zero baseline

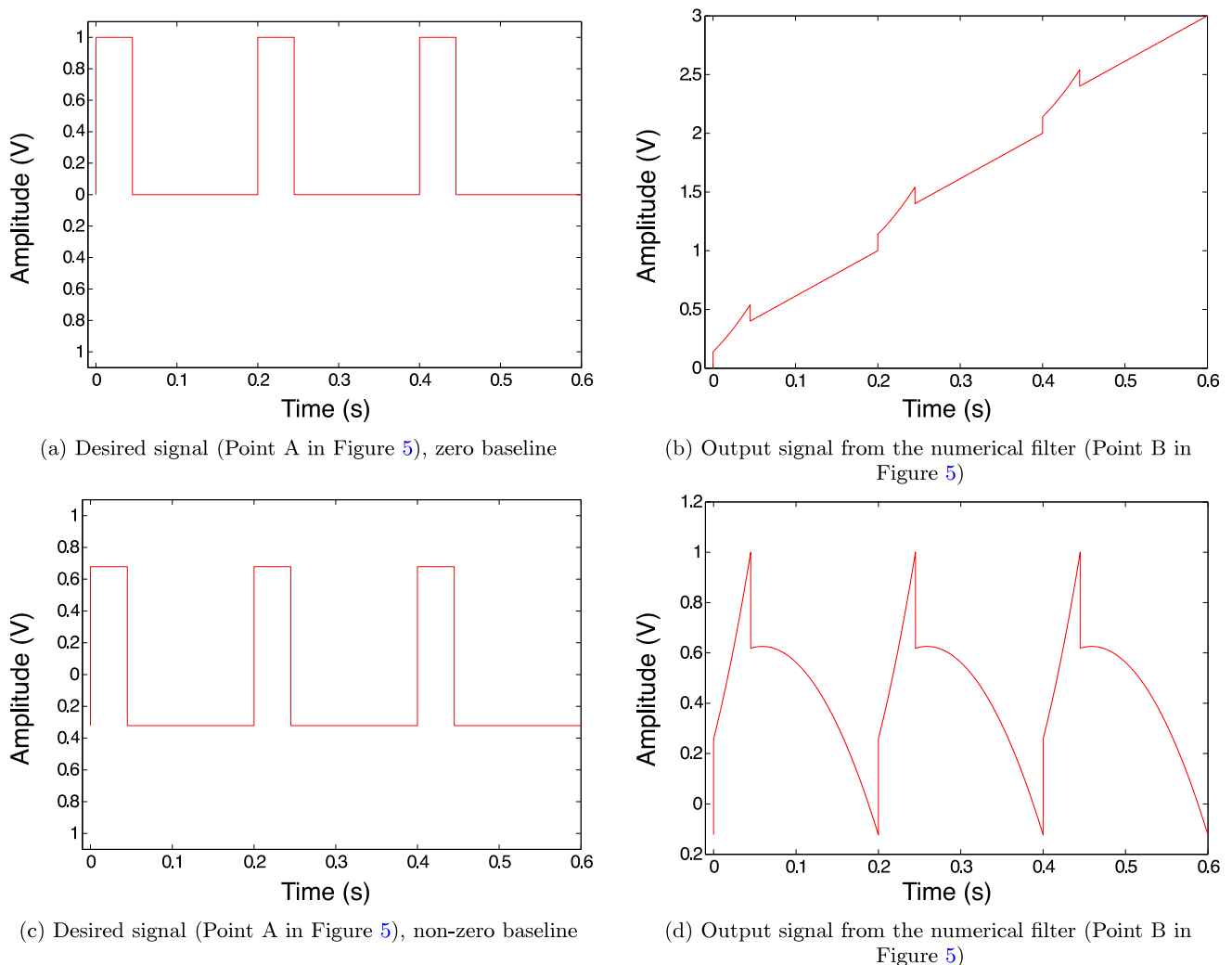(d) Output signal from the numerical filter (Point B in Figure 5)

FIG. 11. Effect of the baseline value of the desired signal on the output signal from the numerical filter.

on the change in voltage rather than the actual voltage applied to the loudspeaker. The aforementioned limitation can therefore be overcome by changing the baseline voltage in the target signal (Fig. 11(c)) in such a way that the average output signal from the numerical filter remains periodic and bounded (Fig. 11(d)). The optimal baseline voltage is determined by minimizing the difference of voltage between the beginning and the end of one drop-generating cycle.

Drops in this study are generated based on an acoustic approach. The drops generated are on the order of μl, much larger than those typically found in commercial inkjet systems, which is on the order of pl. Dimensionless analysis may be applied to generalize the jetting behavior and remove the dependence on the exact drop size. For instance, dimensionless groups, such as Reynolds (Re), Ohnesorge (Oh), and Weber numbers (We), have been successfully used to identify the jettable regime and drop impact characteristics.[4,29–31] However, the relative large drops generated by the current setup also imply that the physics will be dominated by inertia, where splashing and satellite drops are more likely to occur as a result.

V. CONCLUSION

In summary, we demonstrated that a sound card provides a more versatile alternative to generate signals and to control system components. More specifically, an inkjet fluid testing platform was built, where the sound card was successfully applied to (i) generate arbitrary waveforms for drop generation and (ii) to synchronize the drop generation signal with image capturing. A systematic procedure has been developed to characterize the high-pass filters that are commonly built-in to sound cards and amplifiers. Based on the characteristics of the filters, a pre-conditioning numerical filter was created to overcome any associated signal distortions. A mixture of glycerol and water was used as a test fluid to illustrate the capabilities and limitations of the sound-card based system. The sound card used in this paper has a time precision of 5 μs and two channels. As the sound card technology continues to improve, sound cards with a higher time precision and more channels will also become more readily available, opening up the possibilities of controlling multiple components with precision.

[1] I. M. Hutchings and G. D. Martin, *Inkjet Technology for Digital Fabrication* (Wiley, 2012).
[2] P. Calvert, Science **318**, 208 (2007).
[3] S. V. Murphy and A. Atala, Nat. Biotechnol. **32**, 773 (2014).
[4] B. Derby, Annu. Rev. Mater. Res. **40**, 395 (2010).
[5] J. Eggers and E. Villermaux, Rep. Prog. Phys. **71**, 036601 (2008).
[6] L. Rayleigh, Proc. R. Soc. London **29**, 71 (1879).
[7] L. Rayleigh, Philos. Mag. Ser., 5 **34**, 145 (1892).
[8] H. Dong, W. W. Carr, and J. F. Morris, Phys. Fluids **18**, 072102 (2006).
[9] X. Wang, W. W. Carr, D. G. Bucknall, and J. F. Morris, Int. J. Multiphase Flow **38**, 17 (2012).
[10] J. R. Castrejón-Pita, G. D. Martin, S. D. Hoath, and I. M. Hutchings, Rev. Sci. Instrum. **79**, 075108 (2008).
[11] R. J. Furbank and J. F. Morris, Phys. Fluids **16**, 1777 (2004).
[12] R. J. Furbank and J. F. Morris, Int. J. Multiphase Flow **33**, 448 (2007).
[13] A. Lee, H. Jin, H. W. Dang, K. H. Choi, and K. H. Ahn, Langmuir **29**, 13630 (2013).
[14] O. Gennari, L. Battista, B. Silva, S. Grilli, L. Miccio, V. Vespini, S. Coppola, P. Orlando, L. Aprin, P. Slangen, and P. Ferraro, Appl. Phys. Lett. **106**, 054103 (2015).
[15] C. E. Aguiar and M. M. Pereira, Phys. Teacher **49**, 33 (2011).
[16] S. Ganci, Phys. Educ. **43**, 297 (2008).
[17] K. I. Forster and J. C. Forster, Behav. Res. Methods, Instrum., Comput. **35**, 116 (2003).
[18] T. J. Bensky and S. E. Frey, Am. J. Phys. **69**, 1231 (2001).
[19] D. Daineka, P. Bulkin, G. Girard, J.-E. Bourée, and B. Drévillon, Eur. Phys. J. Appl. Phys. **26**, 3 (2004).
[20] Z. Xian-ling, in *2010 International Conference on Computational Aspects of Social Networks* (IEEE, 2010), pp. 743–745.
[21] P. Ferraro, S. Coppola, S. Grilli, M. Paturzo, and V. Vespini, Nat. Nanotechnol. **5**, 429 (2010).
[22] J.-U. Park, M. Hardy, S. J. Kang, K. Barton, K. Adair, D. K. Mukhopadhyay, C. Y. Lee, M. S. Strano, A. G. Alleyne, J. G. Georgiadis, P. M. Ferreira, and J. a. Rogers, Nat. Mater. **6**, 782 (2007).
[23] H. Sirringhaus, T. Kawase, R. H. Friend, T. Shimoda, M. Inbasekaran, W. Wu, and E. P. Woo, Science (New York, N.Y.) **290**, 2123 (2000).
[24] O. Basaran, H. Gao, and P. Bhat, Annu. Rev. Fluid Mech. **45**, 85 (2013).
[25] K. Georgieva, D. J. Dijkstra, H. Fricke, and N. Willenbacher, J. Colloid Interface Sci. **352**, 265 (2010).
[26] S. M. Zakir Hossain, R. E. Luckham, A. M. Smith, J. M. Lebert, L. M. Davies, R. H. Pelton, C. D. M. Filipe, and J. D. Brennan, Anal. Chem. **81**, 5474 (2009).
[27] A. van der Bos, M.-J. van der Meulen, T. Driessen, M. van den Berg, H. Reinten, H. Wijshoff, M. Versluis, and D. Lohse, Phys. Rev. Appl. **1**, 014004 (2014).
[28] I. M. Hutchings, G. D. Martin, and S. D. Hoath, J. Imaging Sci. Technol. **51**, 438 (2007).
[29] B. Derby, J. Eur. Ceram. Soc. **31**, 2543 (2011).
[30] D. Jang, D. Kim, and J. Moon, Langmuir **25**, 2629 (2009).
[31] A. Yarin, Annu. Rev. Fluid Mech. **38**, 159 (2006).